RSC Advances

PAPER

View Article Online
View Journal | View Issue

Cite this: *RSC Adv.*, 2016, **6**, 19089

Influence of silica nanoparticles on mass transfer in a membrane-based micro-contactor†

Seyedeh-Saba Ashrafmansouri,[ab] Stefan Willersinn,[a] Mohsen Nasr Esfahany[b] and Hans-Jörg Bart*[a]

Received 7th December 2015
Accepted 5th February 2016

DOI: 10.1039/c5ra26056f

www.rsc.org/advances

The EFCE (Europ. Fed. Chem. Engng.) extraction test system of toluene–acetone–water was used, where the organic phase was a toluene-based nanofluid containing 0.001 to 0.1 vol% hydrophobic silica nanoparticles. Experiments were performed in a membrane based micro-contactor at various volumetric flow rates of organic and aqueous phases and with a mass transfer direction from the organic to the aqueous phase. The results showed that nanoparticles are more effective on mass transfer at lower flow rates. A maximum enhancement of about 31% in the overall mass transfer coefficient was observed using 0.001 vol% silica nanoparticles. At higher and lower nanoparticle concentrations, smaller extraction efficiencies were observed. Brownian motion of nanoparticles and induced micro-convection is considered to be responsible for observing mass transfer enhancement at low concentrations of nanoparticles. Also, nanoparticle aggregation and reduction in free volume because of the presence of solid nanoparticles is a possibility for deteriorated mass transfer at higher nanoparticle concentrations.

Introduction

Liquid–liquid extraction is an important operation with considerable industrial applications. This process involves the separation of components of a homogeneous liquid by transferring them between contacting immiscible or partially miscible liquids. This technique is used as an energy-saving alternative to distillation in many industrial processes such as the petrochemical, waste water treatment, hydrometallurgical and oil refining industries.[1] There are numerous publications that have dealt with fluid dynamics and mass transfer in liquid–liquid extraction processes. Based on this, fluid dynamics and mass transfer are inseparably linked with interfacial properties and the associated interfacial phenomena, such as droplet deformation, oscillation, Marangoni instabilities, surfactant ad- or desorption, *etc.*[2–4]

Various research groups point out the high potential of micro-structured devices to intensify liquid–liquid extraction processes.[5–8] In micro-process engineering, a higher surface-to-volume ratio and miniaturized length scales lead to shorter diffusion distances, and hence, lower driving forces or shorter contact times are necessary for the same separation task. Although throughput is limited to a few mL min^{-1},[9] the advantages of lower equipment investment, smaller space requirements, lower solvent inventories and safer processing of toxic, explosive or harmful substances[7] compared to conventional extraction equipment may together outweigh this deficiency.[5] Various research on micro-structured liquid–liquid extraction has been reported in the literature on reactive or non-reactive mass transfer, dispersive or non-dispersive flow, different channel geometries, co-current or counter-current flow, *etc.*[5,10–15]

In order to increase the efficiency of a liquid–liquid extraction process recent reports have shown that nanoparticles can enhance mass transfer in liquid–liquid extraction processes.[16–25] Nanofluids have received growing attention because of their proven potential to enhance heat transfer[26–29] with numerous potential applications as super-coolants in nuclear reactors, car engines, radiators, computers, *etc.*[30,31] Here Brownian movement of nanoparticles is considered as one of the major responsible factors in the enhancement of heat transfer. In relation to this, for analogy reasons investigations of mass transfer enhancement in nanofluids with a similar mechanism have been initiated recently.[16,32–36] Investigations in the field of separation processes in the presence of nanoparticles are mostly related to gas absorption processes[37–41] and limited attempts can be found regarding liquid–liquid extraction.[16–25]

Bahmanyar *et al.*[16] investigated the mass transfer performance and hydrodynamic characteristics of kerosene-based SiO_2 nanofluids in a pulsed liquid–liquid extraction column. In their work, the chemical system of kerosene–acetic acid–water was used and the range of SiO_2 nanoparticle concentrations was from 0.01 to 0.1 vol%. They found that the mass transfer coefficient increased by 4 to 60% and static and

[a]*Chair of Separation Science and Technology, University of Kaiserslautern, Kaiserslautern, Germany. E-mail: bart@mv.uni-kl.de; Web: http://www.mv.uni-kl.de/tvt; Fax: +49 (0) 631 205-2119; Tel: +49 (0) 631 205-2414*

[b]*Department of Chemical Engineering, Isfahan University of Technology, Isfahan, Iran*

† Electronic supplementary information (ESI) available. See DOI: 10.1039/c5ra26056f

dynamic dispersed phase hold-ups increased by 23 to 398%, and 23 to 257%, respectively. Khoobi *et al.*[17] investigated the shape of drops, droplet sizes and their distributions under conditions matching those previously reported by Bahmanyar *et al.*[16] They observed that a different content of nanoparticles had a marked influence on the geometrical shapes of the droplets and changed the droplet shape from ellipsoidal to spherical.[17]

Moreover, Ghafoori Roozbahani *et al.*[18] investigated the influence of hydrophobic SiO_2 nanoparticles on the static and dynamic hold-up of the dispersed phase in acetic acid transfer in a pulsed liquid–liquid extraction column. They performed their experiments with kerosene-based dispersions of 0.05 vol% SiO_2 and compared the results obtained in the absence of nanoparticles and in the absence of both nanoparticles and mass transfer, at various pulsation intensities and flow rates. Their results indicated that the presence of nanoparticles increased the dynamic hold-up up to 70% while at the same time decreased the static hold-up in flow rates higher than 70 mL min^{-1} and a pulsation higher than 2.2 cm s^{-1}.

Using an analogy for the heat and mass transfer, Bahmanyar *et al.*[19] recently suggested a model to calculate effective diffusivity and mass transfer coefficients in terms of the nanoparticle volume fraction, Reynolds number, and Schmidt number. They compared the model predictions with their previous experimental data[16] for a pulsed liquid–liquid extraction column. The absolute average relative errors of the proposed model for the mass transfer coefficient and effective diffusivity were 5.3% and 5.4%, respectively.

Mirzazadeh Ghanadi *et al.*[20] investigated the effect of nanoparticles on mass transfer in the liquid–liquid extraction process for the chemical system *n*-butanol–succinic acid–water. They prepared nanofluids with 0.025, 0.05 and 0.1 wt% of ZnO, carbon nanotubes (CNT), and TiO_2 nanoparticles in water. Their results indicated that the effect of ZnO nanoparticles on mass transfer enhancement (up to two-fold) was more than that of CNT and TiO_2 nanoparticles. Furthermore, Mirzazadeh Ghanadi *et al.*[20] observed that mass transfer increased with nanoparticle concentration and the positive effect of the nanoparticles was more distinctive in laminar flow. They found that when the flow mode changes to turbulent flow, as a result of eddy movement, the presence of nanoparticles scarcely influences the mass transfer. Such results can be useful where the capability to manufacture smaller fluidic devices and to quantitatively monitor smaller volumes of liquids bring the process of miniaturization into the domain of laminar flow. New and enabling technologies are being developed using the unique diffusion-based characteristics of the laminar flow domain for sample preparation and analysis. These new analytical systems will have a significant impact on the future of clinical diagnostics.[42]

Nematbakhsh and Rahbar-Kelishami[21] investigated the influence of hydrophobic SiO_2 nanoparticles on mass transfer using an irregularly-packed liquid–liquid extraction column and the chemical system toluene–acetic acid–water. They dispersed nanoparticles with sizes of 10, 30 or 80 nm in toluene–acetic acid to produce nanofluids with different concentrations of 0, 0.01, 0.05 and 0.1 vol%. In their work, the maximum mass transfer coefficient enhancement was approximately 42% at 0.05% concentration of nanoparticles using smaller particles (10 nm).

Saien and Bamdadi[22] investigated the behavior of nanofluid single drops in the liquid–liquid extraction process. In their study, the chemical system of toluene–acetic acid–water was used, and the drops were organic nanofluids containing magnetite or alumina nanoparticles. Saien and Bamdadi[22] examined drop sizes within the range of 2.9 to 4.3 mm, with magnetite and alumina nanoparticle concentrations of 0.0005 to 0.005 wt%. They achieved the maximum mass transfer enhancement at a nanoparticle concentration of 0.002 wt% with enhancement values of 157% and 121% for magnetite and alumina nanoparticles, respectively. They also found that small drops experienced greater mass enhancement but the size of the drops was not found to be influenced much by the nanoparticles.

Recently, Saien *et al.*[23] investigated the influence of an oscillating magnetic field on mass transfer in a magnetite nanofluid single drop liquid–liquid extraction column. They used the chemical system toluene–acetic acid–water, while hydrophobic magnetite nanoparticles were present in the organic dispersed phase. In their work, the magnetic field intensity was within the range of 0.36–1.45 T, accompanied with different nanofluid concentrations within 0.001 to 0.005 wt%. Compared with no magnetic field, an average enhancement of about 65% and a maximum of 121% (for the smallest drops) were achieved in their experiments. They also found that the size of the drops did not vary much with the concentration of nanoparticles.

In our previous articles,[24,25] the influence of toluene-based hydrophobic SiO_2 nanofluids with different nanoparticle concentrations on the mass transfer and hydrodynamics in a spray liquid–liquid extraction column was investigated. Also, the effects of dispersed phase drop sizes and mass transfer direction were evaluated. The results showed that silica nanoparticles have no significant influence on the hydrodynamic parameters, while maximum enhancements of 47% and 107.5% in the overall mass transfer coefficient respectively for mass transfer direction of the dispersed to continuous phase and *vice versa* were achieved for larger drops with 0.001 vol% silica nanoparticles. At higher and lower nanoparticle concentrations, smaller overall mass transfer coefficients were observed.

Until now, the influence of nanoparticles on mass transfer in a micro-extraction process has not been investigated. Many micro-fluidic devices, such as "lab-on-a-chip" types of systems, have limited mass transfer at low Reynolds numbers. If the mass transfer can be improved by passive, nonreacting nanoparticles, a convenient and inexpensive technique to improve the performance of micro-fluidic devices such as micro-extractor systems will be achieved.[32]

In the present work, the influence of hydrophobic silica nanoparticles on the mass transfer in a membrane-based micro-contactor is studied. The extraction test system of toluene–acetone–water proposed by the European Federation of Chemical Engineering (EFCE) is used, and the organic phase is

a toluene-based nanofluid containing 0.001 to 0.1 vol% hydrophobic silica nanoparticles. The experiments are performed at various volumetric flow rates of the organic and aqueous phases and with a mass transfer direction from the organic to the aqueous phase.

Materials and methods

Micro-contactor

The home-made, flat-membrane micro-contactor consists of an upper and a lower basic plate (stainless steel and glass), an upper and a lower channel plate made of polytetrafluoroethylene (thickness: 0.5 mm) with meandering channel geometry (180° U-bends; width: 3 mm) and a porous metal mesh (twilled dutch weave, GKD Geb. Kufferath AG, Dueren, Germany), which separates both micro-channels. The length of each channel was 40.53 cm. Fig. 1 shows the modular design of the micro-contactor (for membrane characteristics see Table 1).

Chemical system and nanofluid preparation

As mentioned above toluene–acetone–water was used in this work. Deionised water was used and as solute, acetone (analytical grade, 99.9%, Merck, Germany) was used, with an initial concentration of 1 wt%. The mass transfer direction was from the organic to aqueous phase, so the solute was dissolved in toluene, technical grade provided by VWR Chemicals (Germany) or toluene-based nanofluids. Hydrophobic silica nanoparticles with an average size of about 14 nm supplied by Plasmachem (Germany) were used to produce nanofluids. An electronic balance (Sartorius research, Germany) accurate to ±0.0001 g was utilized to weigh the required amount of nanoparticles for preparation of a nanofluid with specified concentration.

Nanoparticles were added to toluene by using a digital mixer (IKA RW20, Germany) in 5 min and then sonicated using an ultrasonic system (Laboson 200, Bender & Hobein, Germany) for 20 min. Nanofluids with concentrations of 0.001, 0.01 and 0.1 vol% (0.0025, 0.0254 and 0.2537 wt%) were prepared. To avoid any influence on mass transfer measurements, the colloidal suspension of the concentrated nanofluid was prepared without adding any surfactant and stabilizing agent. Fig. 2 shows the size of the suspended silica nanoparticles, recorded using transmission electron microscopy (TEM). The manufacturer-provided average size of the nanoparticles was confirmed by means of TEM imaging. Since the TEM image was taken 3 h after preparing the nanofluid and the duration of each extraction experiment was shorter than 3 h, nanofluids were stable during the extraction experiments. Moreover, no nanoparticle sedimentation was observed during and after finishing each experiment. Physical properties of the chemical system were measured using a pycnometer, an Ostwald viscometer (CANNON-FENSKE OPAQUE 50, USA) and a tensiometer (Dataphysics, Germany) at 25 °C.

Experimental method

At the beginning of the experiments the organic and aqueous phases were mutually saturated to prevent multi component diffusion processes. First, the apparatus was flooded with the

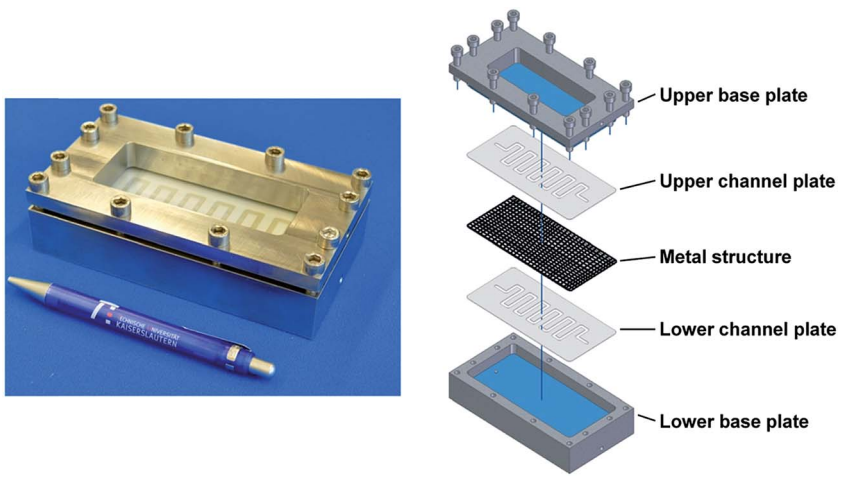

Fig. 1 The modular design of the micro-contactor.[5]

Table 1 Metal structure properties

Name	Material	Thickness[a] δ [μm]	Porosity[a] ε	Av. pore diameter[a] [μm]
Twilled dutch weave	1.4401	67	0.34	9

[a] Manufacturer specification.

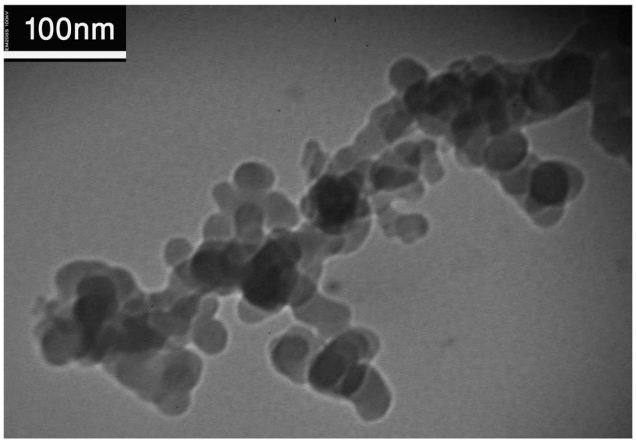

Fig. 2 TEM image of nanofluid.

wetting organic phase using a peristaltic pump (Watson-Marlow 120U DM/2), filling the pores, and then, in counter-current arrangement, the upper channel volume was displaced by the non-wetting aqueous phase using a piston pump (Merck-Hitachi 655 A-12). Therefore, both flow rates could be adjusted independently over a broad range (see Fig. 3). The flow rates were determined gravimetrically. In each experiment, after reaching the steady state, the acetone concentration of the output flow of the aqueous phase was analyzed using gas chromatography (Agilent 6890 Series). Consequently, the organic phase concentrations were determined through mass balance. Each data point is a set of three identical experiments, where the error bars represent the standard deviation. The same procedure was followed for different concentrations of nanoparticles and different organic and aqueous flow rates. In this work, the ratio of volumetric flow rate of the aqueous phase to organic phase was considered within the range of 0.6 to 3. Experiments were done at constant aqueous or organic phase flow rates at 25 °C. The equilibrium experiments were carried out by contacting equal volumes (10 mL) of the aqueous and organic phase at 25 °C for at least 24 h.

Mass transfer calculations

The (average) overall mass transfer coefficient K_{org} (based on the organic phase) was experimentally calculated using the following equation:[43]

$$K_{org} = \frac{Q_{org}(C_{org,0} - C_{org})}{A\Delta C_{LM}} \quad (1)$$

where Q_{org}, $C_{org,0}$, C_{org}, and A are respectively the organic volumetric flow rate, the organic inlet and outlet solute concentrations and the interfacial area between the two phases. Also, the log mean concentration difference ΔC_{LM} over the module for counter-current mode was calculated using eqn (2):[44]

$$\Delta C_{LM} = \frac{(C_{org,0} - D \times C_{aq}) - (C_{org} - C_{aq,0})}{\ln\left(\frac{C_{org,0} - D \times C_{aq}}{C_{org} - C_{aq,0}}\right)} \quad (2)$$

In eqn (2), D, $C_{aq,0}$ and C_{aq} are the distribution coefficient, the aqueous inlet and outlet solute concentration.

The acetone molecules encounter three resistances to mass transfer: the film resistances in the organic and aqueous boundary layers and the membrane resistance. The resistance-in-series model accounts for the mass transfer by integrating these single mass transfer resistances due to diffusion into an overall mass transfer coefficient K_{org}:[44]

$$\frac{1}{K_{org}} = \frac{1}{k_{org}} + \frac{1}{k_m} + \frac{D}{k_{aq}} \quad (3)$$

where k_{org}, k_m and k_{aq} represent the individual mass transfer coefficients for the organic, membrane and aqueous phase, respectively. The experimental overall mass transfer coefficient K_{org} obtained using eqn (1) can be compared with the calculated K_{org} using eqn (3).

In eqn (3), the membrane resistance can be approximated using the membrane properties[44,45] according to eqn (4) and the porosity–tortuosity relationship[46] in eqn (5):

$$k_m = \frac{D_{org}\varepsilon}{\tau\delta} \quad (4)$$

$$\tau = \frac{1}{\varepsilon} \quad (5)$$

In eqn (4), D_{org}, τ, ε and δ are the solute diffusivity in the organic phase, tortuosity, porosity and membrane thickness. Eqn (4) takes the organic diffusion coefficient for a wetting, hydrophobic membrane into account. On the other side, the

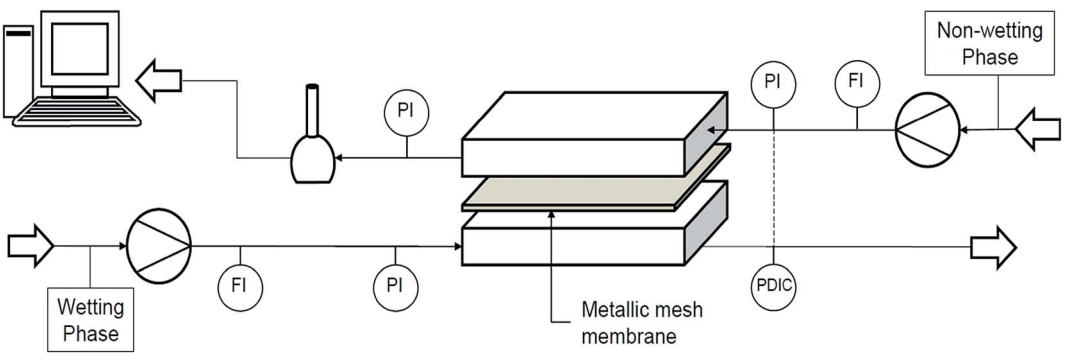

Fig. 3 Process flow sheet for mass transfer studies.[5]

membrane resistance can be experimentally determined using the Wilson-plot method.[44,45,47]

The boundary layer mass transfer coefficients have been extensively studied for laminar flow in hollow fiber membrane contactors[45,48–50] (the well known Lévèque-equation) and to some extent for rectangular micro-channels.[51] The general forms[45,52] of such correlations are given by eqn (6) and (7):

$$\mathrm{Sh}_{\mathrm{aq}} = \frac{k_{\mathrm{aq}} d_{\mathrm{h}}}{D_{\mathrm{aq}}} = a\mathrm{Re}^{b}\mathrm{Sc}^{1/3}\left(\frac{d_{\mathrm{h}}}{L}\right)^{c} \text{ for a water channel} \quad (6)$$

$$\mathrm{Sh}_{\mathrm{org}} = \frac{k_{\mathrm{org}} d_{\mathrm{h}}}{D_{\mathrm{org}}} = a\mathrm{Re}^{b}\mathrm{Sc}^{1/3}\left(\frac{d_{\mathrm{h}}}{L}\right)^{c} \text{ for an organic channel} \quad (7)$$

where d_{h} represents the hydraulic channel diameter, D_{aq} and D_{org} are the diffusion coefficients of the solute in the aqueous and organic phase respectively, the three parameters a, b and c are functions of channel geometry/flow regime and L is the channel length. In eqn (6) and (7), the 1/3-power law of the Schmidt number is generally accepted[5,45] and this power is independent from flow and/or geometry characteristics. In previous studies a mass transfer model was developed (eqn (8) and (9)) for rectangular micro-channels and non-dispersive, membrane-based systems without considering chemical reactions.[5] In the present work, for experiments without nanoparticles, eqn (8) and (9) were used for the aqueous and organic phases.

$$\mathrm{Sh}_{\mathrm{aq}} = \frac{k_{\mathrm{aq}} d_{\mathrm{h}}}{D_{\mathrm{aq}}} = 5.07\mathrm{Re}^{0.27}\mathrm{Sc}^{1/3}\left(\frac{d_{\mathrm{h}}}{L}\right)^{0.44} \text{ for a water channel} \quad (8)$$

$$\mathrm{Sh}_{\mathrm{org}} = \frac{k_{\mathrm{org}} d_{\mathrm{h}}}{D_{\mathrm{org}}} = 5.07\mathrm{Re}^{0.27}\mathrm{Sc}^{1/3}\left(\frac{d_{\mathrm{h}}}{L}\right)^{0.44} \text{ for an organic channel} \quad (9)$$

Since the three parameters a, b and c of eqn (6) and (7) have not yet been optimized for chemical systems including nanoparticles, eqn (8) was only used for an aqueous phase (phase without nanoparticles) and in the organic phase (phase with nanoparticles) the parameters a, b and c of eqn (7) were derived based on the differential evolution (DE) method.[52] Our experimental results showed that eqn (9) is not suitable for chemical systems including nanoparticles and a new set of parameters a, b and c in eqn (7) is required.

Results and discussion

Fig. 4 shows the acetone concentration at different nanoparticle concentrations and aqueous flow rates and at a constant organic flow rate of 0.22 mL min^{-1}. As shown, acetone concentration decreases with the increase in aqueous flow rate of base fluid and nanofluids. In fact, increase in aqueous flow rate causes a decrease in aqueous contact time and as the result lower acetone concentrations in the aqueous phase. Moreover, an increase in aqueous flow rate at constant organic flow rate results in an increase of the operation slope in the operating diagram, with an increase of driving force resulting in a finally lower aqueous phase acetone concentration. This figure also indicates that nanoparticles are more effective at low flow rates and a nanofluid with 0.001 vol% has a more pronounced effect on the acetone concentration profile.

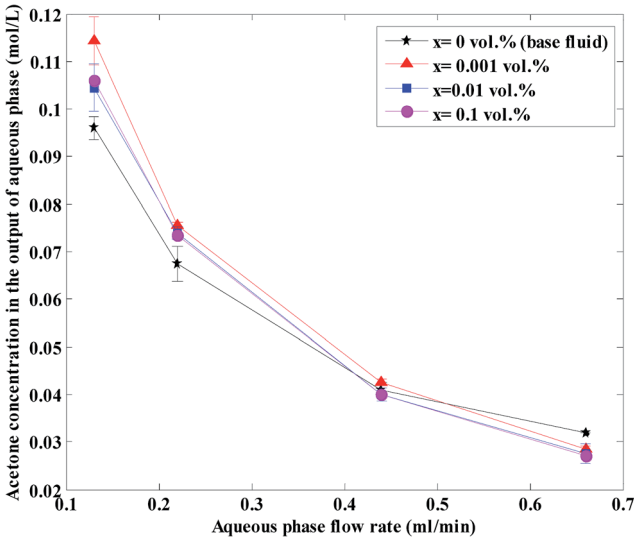

Fig. 4 Aqueous phase acetone concentration in the outlet at different nanoparticle concentrations and at a constant organic flow rate of 0.22 mL min^{-1}.

The overall mass transfer coefficient at different aqueous flow rates and nanoparticle concentrations and at a constant organic flow rate of 0.22 mL min^{-1} is shown in Fig. 5. It is observed that the overall mass transfer coefficient rises with an increase in aqueous flow rate of the base fluid and nanofluids. In this work, the aqueous and organic flow regimes are laminar (most organic and aqueous Reynolds numbers are lower than 10 in the range of the aqueous and organic flow rates used in this work.). In laminar flow, a higher aqueous flow rate facilitates a more enhanced flow profile and thinner boundary layer, which leads to higher overall mass transfer coefficients.

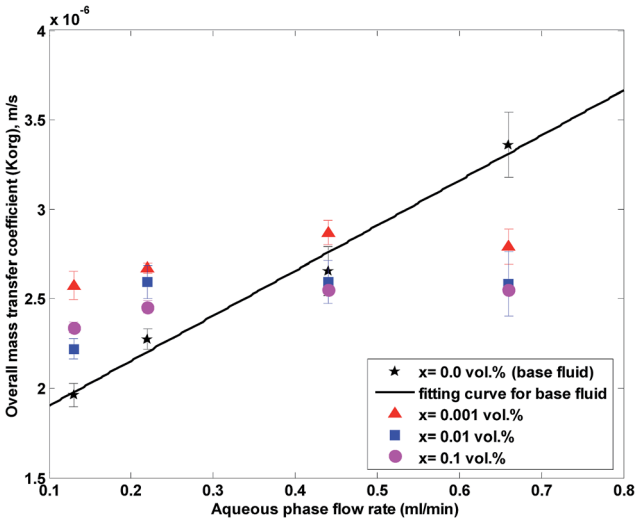

Fig. 5 Overall mass transfer coefficient at different nanoparticle concentrations and at a constant organic flow rate of 0.22 mL min^{-1}.

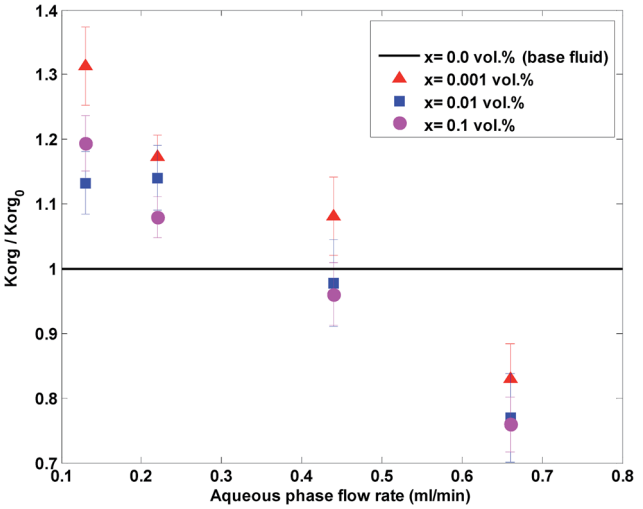

Fig. 6 The ratio of the overall mass transfer coefficient in the nanofluid to the overall mass transfer coefficient in a base fluid at different aqueous flow rates and nanoparticle concentrations.

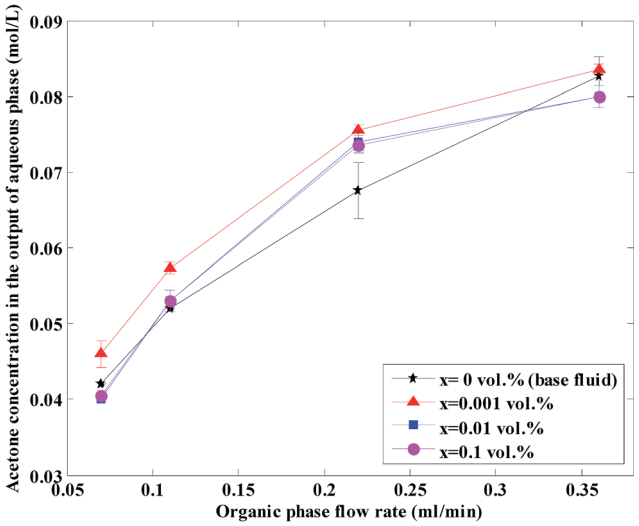

Fig. 7 Acetone concentration at different nanoparticle concentrations and organic flow rates at a constant aqueous flow rate of 0.22 mL min^{-1}.

Fig. 6 shows the ratio of the overall mass transfer coefficient in the nanofluid to the overall mass transfer coefficient in a base fluid (no nanoparticles) at different aqueous flow rates and nanoparticle concentrations and at a constant organic flow rate of 0.22 mL min^{-1}.

Based on Fig. 5 and 6, nanoparticles are more effective at lower flow rates and a nanofluid with 0.001 vol% concentration is more effective on the overall mass transfer coefficient. A maximum enhancement of 31% in the overall mass transfer coefficient is observed at an aqueous flow rate of 0.11 mL min^{-1} and a silica nanoparticle concentration of 0.001 vol%. In fact, a silica nanoparticle concentration of 0.001 vol% is an optimum nanoparticle concentration within the concentration range of 0 to 0.1 vol% and the overall mass transfer coefficient rises to a maximum point for silica nanoparticle concentrations up to 0.001 vol%. A decreasing variation in the overall mass transfer coefficient after this optimum point then occurred upon addition of extra amounts of nanoparticles. To explain the reason for observing this enhancement, some researchers[32,53] believe that Brownian motion of nanoparticles and induced microconvection will increase the mass transfer coefficient. Starting from the generalized Langevin equation, Veilleux and Coulombe[54] showed that the velocity field established around a Brownian nanoparticle is similar to the velocity field predicted by the Brinkman equations leading to the analogy between dispersion in diluted fixed beds and dispersion in nanofluids. Their proposed model predicts the order of magnitude of the mass diffusion enhancement they had observed in their previous work for rhodamine 6G mass diffusivity in water-based alumina nanofluids.[53]

At higher nanoparticle concentrations (higher than 0.001 vol%), with increasing nanoparticle volume fraction, there is a greater likelihood for particle aggregation, producing in effect larger, more massive particles with reduced capacity to promote localized convection.[55] This latter mechanism may be responsible for the decrease after the optimum nanoparticle concentration. In addition to this mechanism, hindrance of diffusion (friction effects with large nanoparticle aggregates) can also be responsible for a decreasing trend after the optimum.[56]

The acetone concentration at the exit in the aqueous phase at different nanoparticle concentrations and organic flow rates is shown in Fig. 7 at a constant aqueous flow rate of 0.22 mL min^{-1}. As shown, the acetone concentration increases with an increase in organic flow rate of the base fluid and nanofluids. In fact, an increase in the organic flow rate at constant aqueous flow rate causes a decrease in the ratio of Q_{aq}/Q_{org} and as a result the slope decreases, thus the driving force decreases and finally the aqueous phase acetone concentration is higher. Based on

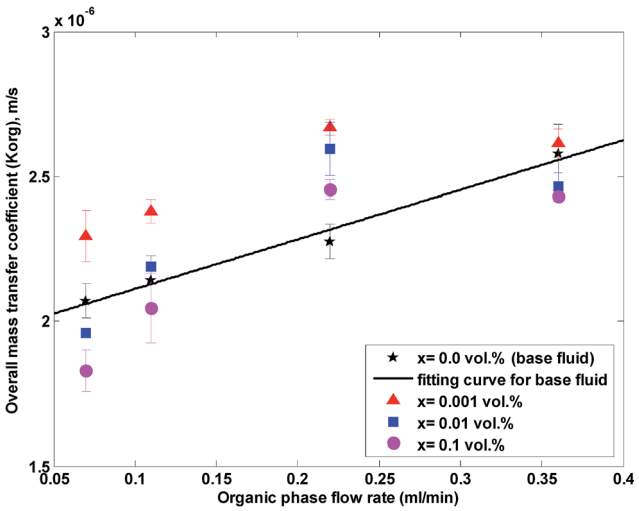

Fig. 8 Overall mass transfer coefficient in a nanofluid at different organic flow rates and nanoparticle concentrations at a constant aqueous flow rate of 0.22 mL min^{-1}.

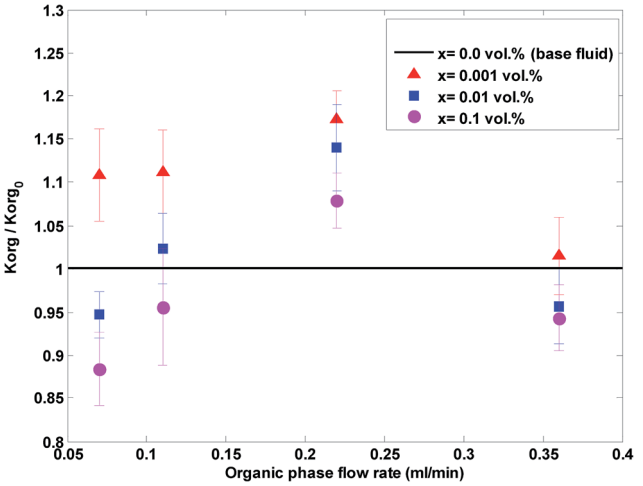

Fig. 9 The ratio of the overall mass transfer coefficient in a nanofluid to the overall mass transfer coefficient in a base fluid at different organic flow rates and nanoparticle concentrations at a constant aqueous flow rate of 0.22 mL min^{-1}.

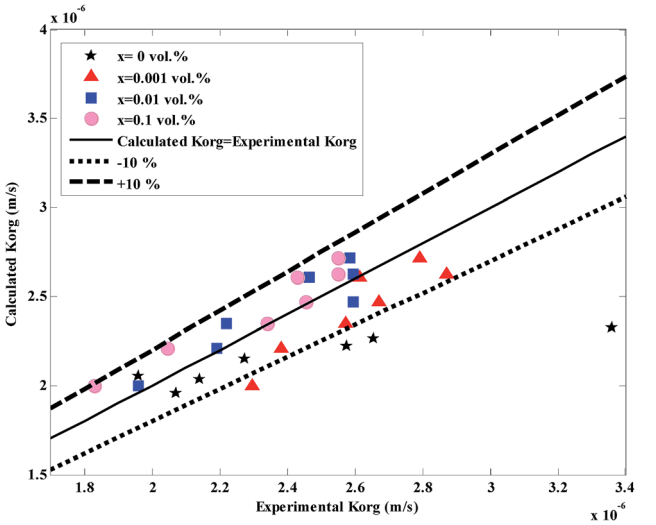

Fig. 10 Comparison between the experimental overall mass transfer coefficient (eqn (1)) and the calculated overall mass transfer coefficient (eqn (3)) (more details of this figure are provided in the ESI†).

this figure, higher effects on the acetone concentration profile are observed at lower organic flow rates for nanofluids with 0.001 vol% concentration.

The overall mass transfer coefficient at different organic flow rates and nanoparticle concentrations and at a constant aqueous flow rate of 0.22 mL min^{-1} is shown in Fig. 8. Similar to Fig. 5, it is observed that the overall mass transfer coefficient rises with an increase in the organic flow rate of the base fluid and nanofluids, because of a more enhanced flow profile and thinner boundary layer at higher organic flow rates. Fig. 9 shows the ratio of the overall mass transfer coefficient in a nanofluid to the overall mass transfer coefficient in a base fluid under these conditions.

As observed in Fig. 8 and 9, higher effects on acetone concentration profile are observed at lower organic flow rates for nanofluids with a 0.001 vol% concentration. A maximum enhancement of 20% in the overall mass transfer coefficient is observed for a silica nanoparticle concentration of 0.001 vol%. Similar to Fig. 5 and 6, a silica nanoparticle concentration of 0.001 vol% is an optimum nanoparticle concentration within the concentration range of 0 to 0.1 vol%.

To compare the experimental overall mass transfer coefficient (K_{org}) obtained based on eqn (1) with literature data, overall mass transfer coefficients at different organic and aqueous flow rates and nanoparticle concentrations were calculated based on eqn (3). For both the base fluid and nanofluids, eqn (8) was used to calculate the individual mass transfer coefficient of the aqueous phase. However, to calculate the individual mass transfer coefficient of the organic phase, eqn (9) was used for experiments with the base fluid and eqn (7) was applied for experiments with nanofluids. For nanofluidic systems the parameters of eqn (7) were optimized based on the DE method and experimental data of the overall mass transfer coefficient. Eqn (10) shows the final optimal results for nanofluids in a micro-contactor system.

$$Sh_{org} = \frac{k_{org} d_h}{D_{org}} = 3.83 Re^{0.78} Sc^{1/3} \left(\frac{d_h}{L}\right)^{0.43} \quad \text{for an organic channel} \tag{10}$$

Fig. 10 shows the values of experimental and calculated mass transfer coefficients at different nanoparticle concentrations and different flow rates. The average of absolute relative deviation between the experimental and calculated overall mass transfer coefficients for the nanofluids and base fluid are respectively 5.14% and 8.25% (without considering the highest experimental value of the overall mass transfer coefficient in Fig. 10). Although some errors for the base fluid are higher than 10%, since these data are based on eqn (9) without any correlation, these errors are acceptable. In addition to this, it is believed that available correlations in the literature underestimate the overall mass transfer coefficients in a micro-structured contactor.[5,57]

Conclusions

In the present work, the influence of hydrophobic silica nanoparticles on mass diffusion in a membrane-based micro-contactor was studied. The chemical system of toluene–acetone–water proposed by the European Federation of Chemical Engineering (EFCE) was used, and the organic phase was a toluene-based nanofluid containing 0.001 to 0.1 vol% hydrophobic silica nanoparticles. The experiments were performed at various volumetric flow rates of organic and aqueous phases and with a mass transfer direction from the organic to the aqueous phase.

The results showed that nanoparticles are more effective on mass transfer at low flow rates. A maximum enhancement of about 31% in the overall mass transfer coefficient was observed using 0.001 vol% of silica nanoparticles. At higher and lower

nanoparticle concentrations, smaller extraction efficiencies were observed. Experimental overall mass transfer coefficients were in good agreement with calculated overall mass transfer coefficients based on literature equations. Brownian motion of nanoparticles and induced micro-convection could be responsible for observing mass transfer enhancements at low concentrations of nanoparticles. Also, nanoparticle aggregation and hindered diffusion (friction with nanoparticle aggregates) of the solute could be responsible for deteriorated mass transfer at higher nanoparticle concentrations.

References

1 A. Javadi, D. Bastani and M. Taeibi-Rahni, *AIChE J.*, 2006, **52**(3), 895–910.
2 M. Wegener, N. Paul and M. Kraume, *Int. J. Heat Mass Transfer*, 2014, **71**, 475–495.
3 M. Wegener, *Int. J. Heat Mass Transfer*, 2014, **71**, 769–778.
4 M. Wegener and A. R. Paschedag, *Int. J. Heat Mass Transfer*, 2012, **55**, 1561–1573.
5 S. Willersinn and H.-J. Bart, *Chem. Eng. Process.*, 2015, **95**, 186–194.
6 N. Kockmann, J. Kussi, G. Schembecker, V. Hessel, I. V. Gürsel and Q. Wang, *Chem. Ing. Tech.*, 2012, **84**(5), 660–684.
7 J.-C. Charpentier, *Chem. Eng. J.*, 2007, **134**(1–3), 84–92.
8 E. Y. Kenig, Y. Su, A. Lautenschleger, P. Chasanis and M. Grünewald, *Sep. Purif. Technol.*, 2013, **120**, 245–264.
9 V. Hessel, A. Renken, J. C. Schouten and J. Yoshida, *Micro Process Engineering*, Wiley-VCH Weinheim, 2009.
10 K. P. Nichols, R. R. Pompano, L. Li, A. V. Gelis and R. F. Ismagilov, *J. Am. Chem. Soc.*, 2011, **133**(39), 15721–15729.
11 D. Ciceri, J. M. Perera and G. W. Stevens, *Microfluid. Nanofluid.*, 2011, **11**(5), 593–600.
12 M. Darekar, N. Sen, K. K. Singh, S. Mukhopadhyay, K. T. Shenoy and S. K. Ghosh, *Hydrometallurgy*, 2014, **144–145**, 54–62.
13 J. Hereijgers, M. Callewaert, X. Lin, H. Verelst, T. Breugelmans and H. Ottevaere, *J. Membr. Sci.*, 2013, **436**, 154–162.
14 M. B. Mansur, M. J. Slater and E. C. Biscaia, *Hydrometallurgy*, 2002, **63**(2), 107–116.
15 J. Hereijgers, N. van Oeteren, J. F. M Denayer and T. Breugelmans, *Chem. Eng. J.*, 2015, **273**, 138–146.
16 A. Bahmanyar, N. Khoobi, M. R. Mozdianfard and H. Bahmanyar, *Chem. Eng. Process.*, 2011, **50**, 1198–1206.
17 N. Khoobi, A. Bahmanyar, H. Molavi, D. Bastani, M. R. Mozdianfard and H. Bahmanyar, *Can. J. Chem. Eng.*, 2013, **91**(3), 506–515.
18 M. A. Ghafoori Roozbahani, M. Sattari Najafabadi, K. Nazari Hassan Abadi and H. Bahmanyar, *Chem. Eng. Commun.*, 2015, **202**(11), 1468–1477.
19 A. Bahmanyar, N. Khoobi, M. Mohammad Ali Moharrer and H. Bahmanyar, *Chem. Eng. Res. Des.*, 2014, **92**(11), 2313–2323.
20 A. Mirzazadeh Ghanadi, A. Heydari Nasab, D. Bastani and A. K. Seife Kordi, *Chem. Eng. Commun.*, 2015, **202**(5), 600–605.
21 G. Nematbakhsh and A. Rahbar-Kelishami, *Chem. Eng. Commun.*, 2014, **202**(11), 1493–1501.
22 J. Saien and H. Bamdadi, *Ind. Eng. Chem. Res.*, 2012, **51**, 5157–5166.
23 J. Saien, H. Bamdadi and S. Daliri, *J. Ind. Eng. Chem.*, 2015, **21**, 1152–1159.
24 S. S. Ashrafmansouri and M. Nasr Esfahany, *Sep. Purif. Technol.*, 2015, **151**, 74–81.
25 S. S. Ashrafmansouri and M. Nasr Esfahany, *AIChE J.*, 2015, DOI: 10.1002/aic.15084, accepted.
26 S. U. S. Choi, *J. Heat Transfer*, 2009, **131**(3), 1–9.
27 P. Keblinski, J. A. Eastman and D. G. Cahill, *Mater. Today*, 2005, **8**, 36–44.
28 J. Buongiorno, *J. Heat Transfer*, 2006, **128**(3), 240–250.
29 F. Asadzadeh, M. Nasr Esfahany and N. Etesami, *Int. J. Therm. Sci.*, 2012, **62**, 114–119.
30 S. Ozturk, A. Y. Hassan and V. M. Ugaz, *Nano Lett.*, 2010, **10**, 665–671.
31 H. A. Mohammed, A. A. Al-aswadi, N. H. Shuaib and R. Saidur, *Renewable Sustainable Energy Rev.*, 2011, **15**, 2921–2939.
32 S. Krishnamurthy, P. Bhattacharya, P. E. Phelan and R. S. Prasher, *Nano Lett.*, 2006, **6**(3), 419–423.
33 N. Keshishian, M. Nasr Esfahany and N. Etesami, *Int. Commun. Heat Mass Transfer*, 2013, **46**, 148–153.
34 H. Beiki, M. Nasr Esfahany and N. Etesami, *Microfluid. Nanofluid.*, 2013, **15**(4), 501–508.
35 H. Beiki, M. Nasr Esfahany and N. Etesami, *Int. J. Therm. Sci.*, 2013, **64**, 251–256.
36 S. S. Ashrafmansouri and M. Nasr Esfahany, *Int. J. Therm. Sci.*, 2014, **82**, 84–99.
37 B. Olle, S. Bucak, T. C. Holmes, L. Bromberg, T. A. Hatton and D. I. C. Wang, *Ind. Eng. Chem. Res.*, 2006, **45**, 4355–4363.
38 E. Nagy, T. Feczkó and B. Koroknai, *Chem. Eng. Sci.*, 2007, **62**, 7391–7398.
39 J. Y. Jung, J. W. Lee and Y. T. Kang, *J. Mech. Sci. Technol.*, 2012, **26**(8), 2285–2290.
40 H. Kim, J. Jeong and Y. T. Kang, *Int. J. Refrig.*, 2012, **35**(3), 645–651.
41 S. H. EsmaeiliFaraj, M. Nasr Esfahany, M. Jafari-Asl and N. Etesami, *Ind. Eng. Chem. Res.*, 2014, **53**(43), 16851–16858.
42 T. H. Schulte, R. L. Bardell and B. H. Weigl, *Clin. Chim. Acta*, 2002, **321**(1–2), 1–10.
43 R. Prasad and K. K. Sirkar, Membrane based Solvent Extraction, in *Membrane Handbook*, Van Nostrand Reinhold, New York, 1992, pp. 727–763.
44 A. Gabelman and S. T. Hwang, *J. Membr. Sci.*, 1999, **159**, 61–106.
45 R. Viegas, M. Rodriguez, S. Luque, J. Alvarez, I. Coelhoso and J. Crespo, *J. Membr. Sci.*, 1998, **145**, 129–142.
46 S. B. Iversen, V. K. Bhatia, K. Dam-Johansen and G. Jonsson, *J. Membr. Sci.*, 1997, **130**, 205–217.
47 E. E. Wilson, *Trans. ASME*, 1915, **37**, 47.

48 R. O. Crowder and E. L. Cussler, *J. Membr. Sci.*, 1998, **145**, 173–184.
49 C. Yang and E. L. Cussler, *Biotechnol. Bioeng.*, 2000, **69**, 66–73.
50 E. A. Fouad and H.-J. Bart, *J. Membr. Sci.*, 2008, **307**(2), 156–168.
51 P. van Male, M. H. J. M. de Croon, R. M. Tiggelaar, A. van den Berg and J. C. Schouten, *Int. J. Heat Mass Transfer*, 2004, **47**(1), 87–99.
52 B. V. Babu and R. Angira, *Comput. Chem. Eng.*, 2006, **30**, 989.
53 J. Veilleux and S. A. Coulombe, *J. Appl. Phys.*, 2010, **108**, 104316.
54 J. Veilleux and S. A. Coulombe, *Chem. Eng. Sci.*, 2011, **66**, 2377–2384.
55 X. Fang, Y. Xuan and Q. Li, *Appl. Phys. Lett.*, 2009, **95**, 203108.
56 C. Gerardi, D. Cory, J. Buongiorno, L. W. Hu and T. McKrell, *Appl. Phys. Lett.*, 2009, **95**, 253104.
57 S. Willersinn and H.-J. Bart, *Proceedings ISEC2014, 7–11.09.2014, Würzburg*, ed. DECHEMA, Frankfurt, 2014, BRD.